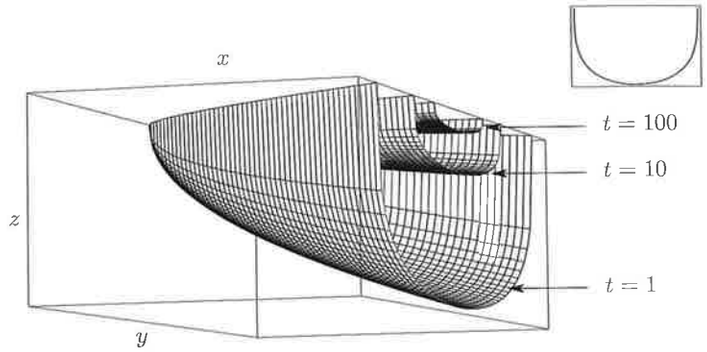

Fig. 4. As in Fig. 3, but with $H_0 = H_{02}$

The alternative choice $S_t = -1$, $S_g = 1$, $S_x = -1$ leads to exactly the same mathematical problem as that discussed above, but the physical interpretation is rather different, since it corresponds to sessile rivulets in $x < 0$, with $t < 0$. At any time t (< 0) the rivulets become thinner and narrower with increasing x (< 0), but at any x (< 0) they become wider and thicker as time elapses. In fact, in this interpretation the solutions exhibit a finite-time singularity, at $t = 0$, with h becoming infinite everywhere then.

There remains the question of whether rivulet solutions of the above types could occur in practice. In particular, the stability of the solutions is, of course, crucial, but it seems that even a restricted linear stability analysis is likely to be a formidable task.

Acknowledgement

The first author (YMY) wishes to thank the Ministry of Higher Education, Malaysia and University of Science, Malaysia for financial support via an Academic Staff Training Fellowship.

References

1. Duffy, B.R., Moffatt, H.K.: Euro. J. Appl. Math. **8**, 37–47 (1997)
2. Huppert, H.E.: J. Fluid Mech. **121**, 43–58 (1982)
3. Huppert, H.E.: Nature **300**, 427–429 (1982)
4. Lister, J.R.: J. Fluid Mech. **242**, 631–653 (1992)
5. Pattle, R.E.: Q. Jl Mech. Appl. Math. **12**, 407–409 (1959).
6. Smith, P.C.: J. Fluid Mech. **58**, 275–288 (1973)
7. Smith, S.H.: J. Appl. Math. Phys. **20**, 556–560 (1969)
8. Wilson, S.K., Duffy, B.R.: J. Engng. Math. **42**, 359–372 (2002)
9. Wilson, S.K., Duffy, B.R., Hunt, R.: Q. Jl Mech. Appl. Math. **55**, 385–408 (2002)
10. Zel'dovich, Ya.B., Kompaneets, A.S.: Izv. Akad. Nauk SSSR 61–71 (1950)

Depinning of 2d and 3d Droplets Blocked by a Hydrophobic Defect

P. Beltrame[1,2], P. Hänggi[1], E. Knobloch[3], and U. Thiele[4]

[1] Institut für Physik, Universität Augsburg, D-86135 Augsburg, Germany
Philippe.Beltrame@avignon.inra.fr,
Peter.Hanggi@physik.uni-augsburg.de
[2] Dept. de Physique, Universite d'Avignon, F-84000 Avignon, France
[3] Department of Physics, University of California, Berkeley CA 94720, USA
knobloch@berkeley.edu
[4] Department of Mathematical Sciences, Loughborough University, Loughborough, Leicestershire, LE11 3TU, UK u.thiele@lboro.ac.uk

Summary. On non-ideal real substrates the onset of droplet motion under lateral driving is strongly influenced by substrate defects. A finite driving force is necessary to overcome the pinning influence of microscale heterogeneities. The dynamics of depinning two- and three-dimensional droplets is studied using a long-wave evolution equation for the film thickness profile in the case of a localized hydrophobic wettability defect. It is found that the nature of the depinning transition explains the experimentally observed stick-slip motion.

1 Introduction

Both steady states and the evolution in time of droplets or liquid films on solid substrates in the limit of small contact angles and surface slopes are described well by the thin film or lubrication equation [13, 19]

$$\partial_t h = -\nabla \cdot [m(h)\nabla p(h) + \mu(h)\mathbf{e_x}], \qquad (1)$$

where $h(x, y, t)$ is the thickness profile, $m(h)$ is the mobility, and $\mu(h)$ represents a lateral driving force.

For a droplet on an incline this force might be due to gravity. In other situations similar forces arise as the result of rotation (centrifugal force), or gradients in wettability, although temperature and electrical field gradients can also introduce lateral forces into the problem. The pressure $p(h)$ may contain several terms, e.g., curvature pressure (capillary) or a thickness-dependent disjoining pressure $\Pi(h)$ modeling the effective molecular interactions between substrate and film surface (wettability), for example, due to van der Waals interactions [5, 12]. Other contributions may arise from electrostatic fields [16, 18, 38], thermal effects [2, 20, 37] or hydrostatics [4, 6, 9].

A.D. Fitt et al. (eds.), *Progress in Industrial Mathematics at ECMI 2008*,
Mathematics in Industry 15, DOI 10.1007/978-3-642-12110-4_99,

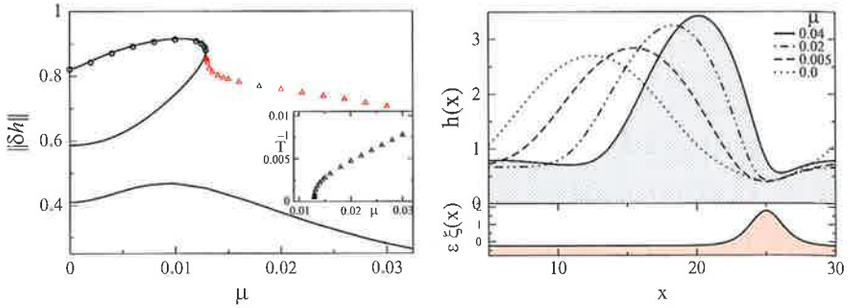

Fig. 1. (**a**) Bifurcation diagram for a droplet that depins via a sniper bifurcation. The localized hydrophobic defect with $s = 6$, $\epsilon = 0.4$ and $b = 0.1$ pins the droplet until depinning occurs at the lateral driving force $\mu_c \approx 0.014$. For details see main text. (**b**) Thickness profiles of pinned droplets for $\mu < \mu_c$ for $\epsilon = 1$. The lower panel gives the profile of the heterogeneity $\xi(x)$. The domain size is $L = 25$ and the liquid volume is $V = 37.5$

The system behavior is well studied for smooth homogeneous substrates. Without lateral driving force, an unstable film may structure via a long-wave instability resulting in patterns of holes, drops or labyrinths. The emerging structure sizes depend on the mean film thickness and the type of destabilizing influence [2, 23, 26, 27, 29]. One finds a similar situation for systems involving lateral driving forces such as gravity for a film on an incline [11,21]. The lateral driving gives rise to phenomena like transverse front instabilities [8,11,28,31]. A few studies focus on films and drops on heterogeneous substrates without lateral driving [3,14,30]. However, relatively little is known about the interplay of lateral driving and substrate heterogeneities. This is an important problem as such heterogeneities may cause stick-slip motion [25] or roughening [10, 24] of moving contact lines, and are thought to be responsible for contact angle hysteresis [5, 15, 22].

Recently, [32, 33] studied the problem employing a dynamical systems approach based on thin film theory. In particular they use a wettability (disjoining pressure) that depends on the location on the substrate. In this way localized hydrophilic or hydrophobic substrate defects can be modeled. Constructing an idealized periodically heterogeneous substrate one can then employ tools of dynamical systems theory to study steady droplet constellations under small driving and the dynamics of the depinning process at a larger lateral driving. The dynamical approach has the advantage over static variational methods [17] in that it allows one to investigate the evolution of droplet shapes and stability as a function of the driving and the dynamics of the depinning process itself. In the following we will present a selection of results on the depinning of 2d droplets [33] and add material for the depinning of 3d droplets pinned by a line defect. As an example we use a hydrophobic defect that blocks the droplet at its front. For the case of a hydrophilic defect we refer to [1, 32, 33].

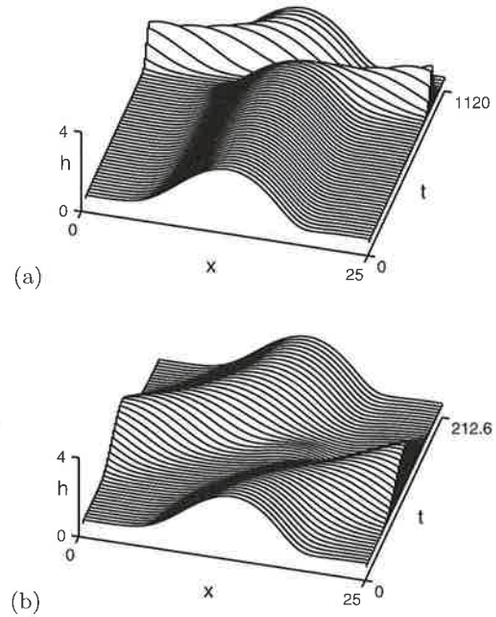

Fig. 2. The droplet dynamics beyond depinning is shown as space-time plot for one period in space and time (**a**) close to depinning at $\mu = 0.013$ with a temporal period of $T = 1119.9$, and (**b**) far from depinning at $\mu = 0.02$ ($T = 212.6$). The remaining parameters are as in Fig. 1a

2 Model

To model a wettability defect we let the short-range part of the disjoining pressure Π depend on the coordinate x (using expressions as in [33]). The resulting film evolution equation in dimensionless form for 3d droplets is

$$\partial_t h = -\nabla \cdot \left\{ h^3 \left[\nabla \left(\Delta h + \Pi(h, x) \right) + \mu \mathbf{e_x} \right] \right\}, \tag{2}$$

where

$$\Pi(h, x) = \frac{b}{h^3} - \left[1 + \epsilon \xi(x) \right] e^{-h} \tag{3}$$

is the dimensionless disjoining pressure (for details see [33, 35]). We chose $\xi(x) = \{2\,\mathrm{cn}[2K(k)x/L, k]\}^2 - \Delta$ with $K(k)$ being the complete elliptic integral of the first kind and Δ is either zero or chosen in such a way that the average of $\xi(x)$ is zero. L is the system size. For $k = 0$ the profile is sinusoidal whereas for $k \to 1$ one obtains for $\epsilon > 0$ localized hydrophobic defects. We further introduce the logarithmic measure $s \equiv -\log(1 - k)$.

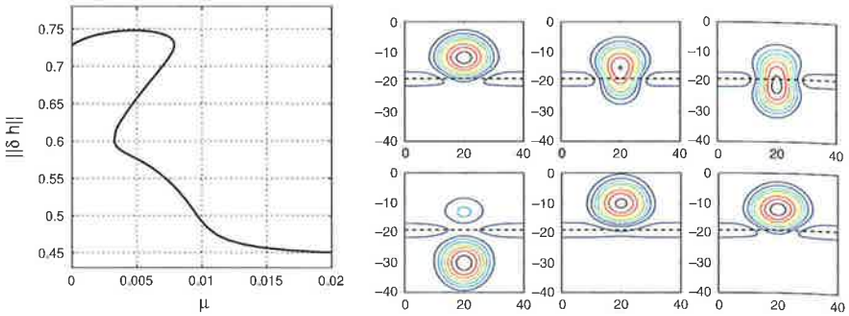

Fig. 3. (**a**) Bifurcation diagram for a 3d droplet for increasing lateral driving force μ and $\epsilon = 0.3$. The steady droplet solutions are characterized by their L^2 norm $||\delta h||$. (**b**) Shown are snapshots of height contour lines characterizing the droplet dynamics beyond their depinning via a sniper bifurcation for $\mu = 8.0 \times 10^{-3}$. From *top left* to *bottom right* droplets are shown at times $t = 0, 1160, 1240, 1340, 1680, 2930$. The position of the line defect is indicated by a *straight horizontal line*. The domain size is 40×40, $V = 1600$, and the distance between the contour lines $\Delta h = 0.4$

3 Results

Under lateral driving ($\mu > 0$) no droplet remains at rest on a homogeneous substrate ($\epsilon = 0$), i.e., a substrate without lateral variation or defect. All such droplets will (in the lubrication limit) slide with a constant velocity that is determined by the driving force, the properties of the liquid, and the wettability [34, 36]. The situation is very different on a heterogeneous substrate. There drops are pinned for small driving, and depin at a critical driving μ_c. For larger driving the droplets slide with a profile that is modulated when passing a defect.

Figure 1a presents the corresponding bifurcation diagram. It gives as solid line the L^2 norm for steady droplet solutions obtained by continuation [7], selected steady solutions as obtained by time integration (circles) and the time-averaged L^2 norm for the unsteady sliding droplet solutions beyond depinning (triangles). The inverse time period for the latter is given as inset. Its $(\mu - \mu_c)^{1/2}$ dependence indicates that the bifurcation represents a Saddle Node Infinite PERiod (SNIPER) bifurcation. Selected steady profiles before depinning ($\mu < \mu_c$) are shown in Fig. 1b. The time evolution beyond depinning is represented in the form of space-time plots for a typical stick-slip motion close to the sniper bifurcation (Fig. 2a) and for a larger force where droplet motion is more continuous (Fig. 2b).

Recently a path-following algorithm has been developed for three-dimensional droplets [1]. It has been shown that all main results on depinning obtained for 2d droplets hold as well for 3d droplets. Figure 3a shows the bifurcation diagram for a single droplet on a square domain blocked by a

hydrophobic stripe-like defect. It strongly resembles the corresponding result for the 2d case (Fig. 1a). Time simulations show that depinning occurs via a SNIPER bifurcation in this case as well. An example of a time series for a stick-slip motion of a single droplet is given in Fig. 3b as a series of snapshots. Note that the times at which the snapshots are taken are not equidistant. It takes the droplet about 1200 time units to slowly let an advancing 'protrusion' creep over the defect (snapshot 1–2). Then within 500 units it depins and slides to the next defect (snapshot 2–5), where it needs another 1300 units to reach again the same state as in snapshot 1 (snapshot 5–6). All together for the chosen value of μ the ratio of stick phase to slip phase is about 5:1. The ratio becomes larger if one approaches the bifurcation point.

4 Conclusion

We have reviewed recent work on the depinning dynamics of the depinning of two- and three-dimensional droplets under lateral driving. Here, we have focused on one type of defect (hydrophobic, localized) and one type of depinning transition (SNIPER). For results on hydrophilic defects and for larger drops see [1, 32, 33].

We have found that the depinning behavior is very similar for 2d and 3d droplets: Droplets are pinned up to a critical driving strength μ_c where they depin via a SNIPER bifurcation characterized by a square-root dependence of the inverse time scale of depinning on the distance $\mu - \mu_c$. Slightly above the bifurcation the unsteady motion resembles the stick-slip motion observed in experiment: The advancing motion is extremely slow when the drop 'creeps' over a hydrophobic defect, and very fast once the drop breaks away from the defect and slides to the next one. The difference in time scales for the stick- and the slip-phase can be many orders of magnitude.

Note that at very large driving depinning might as well occur via a Hopf instead of a SNIPER bifurcation [32]. It is thought that then the depinning is actually caused by the flow in the wetting layer, an effect that will for realistic forces not be observed for partially wetting nano- or micro-droplets on an incline with wettability defects. However, for dielectric liquids a thick wetting layer of 100 nm to 1 μm stabilized by van der Waals interaction can coexist with micro-droplets generated by an electric field [16, 18], and both depinning mechanisms should be observable using gravity as the driving force (see appendix of [33]).

We acknowledge support by the EU [MRTN-CT-2004005728 PATTERNS] and the DFG [SFB 486, project B13].

References

1. Beltrame, P., Thiele, U.: SIAM J. Applied Dynamical Systems, (2010) (at press)
2. Bestehorn, M., Pototsky, A., Thiele, U.: Eur. Phys. J. B **33**, 457–467 (2003)
3. Brinkmann, M., Lipowsky, R.: J. Appl. Phys. **92**, 4296–4306 (2002)
4. Burgess, J.M., Juel, A., McCormick, W.D., Swift, J.B., Swinney, H.L.: Phys. Rev. Lett. **86**, 1203–1206 (2001)
5. de Gennes, P.-G.: Rev. Mod. Phys. **57**, 827–863 (1985)
6. Deissler, R.J., Oron, A.: Phys. Rev. Lett. **68**, 2948–2951 (1992)
7. Doedel, E.J., Champneys, A.R., Fairgrieve, T.F., Kuznetsov, Y.A., Sandstede, B., Wang, X.J.: AUTO97: Continuation and bifurcation software for ordinary differential equations. Concordia University, Montreal (1997)
8. Eres, M.H., Schwartz, L.W., Roy, R.V.: Phys. Fluids **12**, 1278–1295 (2000)
9. Fermigier, M., Limat, L., Wesfreid, J.E., Boudinet, P., Quilliet, C.: J. Fluid Mech. **236**, 349–383 (1992)
10. Golestanian, R., Raphaël, E.: Europhys. Lett. **55**, 228–234 (2001)
11. Huppert, H.E.: Nature **300**, 427–429 (1982)
12. Israelachvili, J.N.: Intermolecular and Surface Forces. Academic, London (1992)
13. Kalliadasis, S., Thiele, U. (eds.) Thin Films of Soft Matter. Springer, Wien (2007)
14. Konnur, R., Kargupta, K., Sharma, A.: Phys. Rev. Lett. **84**, 931–934 (2000)
15. Leger, L., Joanny, J.F.: Rep. Prog. Phys. **55**, 431–486 (1992)
16. Lin, Z., Kerle, T., Baker, S.M., Hoagland, D.A., Schäffer, E., Steiner, U., Russell, T.P.: J. Chem. Phys. **114**, 2377–2381 (2001)
17. Marmur, A.: Colloid Surf. A-Physicochem. Eng. Asp. **116**, 55–61 (1996)
18. Merkt, D., Pototsky, A., Bestehorn, M., Thiele, U.: Phys. Fluids **17**, 064104 (2005)
19. Oron, A., Davis, S.H., Bankoff, S.G.: Rev. Mod. Phys. **69**, 931–980 (1997)
20. Oron, A., Rosenau, P.: J. Fluid Mech. **273**, 361–374 (1994)
21. Podgorski, T., Flesselles, J.-M., Limat, L.: Phys. Rev. Lett. **87**, 036102 (2001)
22. Quéré, D., Azzopardi, M.J., Delattre, L.: Langmuir **14**, 2213–2216 (1998)
23. Reiter, G.: Phys. Rev. Lett. **68**, 75–78 (1992)
24. Robbins, M.O., Joanny, J.F.: Europhys. Lett. **3**, 729–735 (1987)
25. Schäffer, E., Wong, P.Z.: Phys. Rev. Lett. **80**, 3069–3072 (1998)
26. Seemann, R., Herminghaus, S., Neto, C., Schlagowski, S., Podzimek, D., Konrad, R., Mantz, H., Jacobs, K.: J. Phys.-Condes. Matter **17**, S267–S290 (2005)
27. Sharma, A., Khanna, R.: Phys. Rev. Lett. **81**, 3463–3466 (1998)
28. Spaid, M.A., Homsy, G.M.: Phys. Fluids **8**, 460–478 (1996)
29. Thiele, U.: Eur. Phys. J. E **12**, 409–416 (2003)
30. Thiele, U., Brusch, L., Bestehorn, M., Bär, M.: Eur. Phys. J. E **11**, 255–271 (2003)
31. Thiele, U., Knobloch, E.: Phys. Fluids **15**, 892–907 (2003)
32. Thiele, U., Knobloch, E.: Phys. Rev. Lett. **97**, 204501 (2006)
33. Thiele, U., Knobloch, E.: New J. Phys. **8**(313), 1–37 (2006)
34. Thiele, U., Neuffer, K., Bestehorn, M., Pomeau, Y., Velarde, M.G.: Colloid Surf. A **206**, 87–104 (2002)
35. Thiele, U., Velarde, M.G., Neuffer, K.: Phys. Rev. Lett. **87**, 016104 (2001)

36. Thiele, U., Velarde, M.G., Neuffer, K., Bestehorn, M., Pomeau, Y.: Phys. Rev. E **64**, 061601 (2001)
37. VanHook, S.J., Schatz, M.F., Swift, J.B., McCormick, W.D., Swinney, H.L.: J. Fluid Mech. **345**, 45–78 (1997)
38. Verma, R., Sharma, A., Kargupta, K., Bhaumik, J.: Langmuir **21**, 3710–3721 (2005)